



Accelerated Degradation in a Quasi-Single-Crystalline Layered Oxide Cathode for Lithium-Ion Batteries Caused by Residual Grain Boundaries

R. Zhang, M. Ge

To be published in "NANO LETTERS"

May 2022

Photon Sciences

Brookhaven National Laboratory

U.S. Department of Energy

USDOE Office of Science (SC), Basic Energy Sciences (BES) (SC-22)

Notice: This manuscript has been authored by employees of Brookhaven Science Associates, LLC under Contract No.DE-SC0012704 with the U.S. Department of Energy. The publisher by accepting the manuscript for publication acknowledges that the United States Government retains a non-exclusive, paid-up, irrevocable, world-wide license to publish or reproduce the published form of this manuscript, or allow others to do so, for United States Government purposes.

DISCLAIMER

This report was prepared as an account of work sponsored by an agency of the United States Government. Neither the United States Government nor any agency thereof, nor any of their employees, nor any of their contractors, subcontractors, or their employees, makes any warranty, express or implied, or assumes any legal liability or responsibility for the accuracy, completeness, or any third party's use or the results of such use of any information, apparatus, product, or process disclosed, or represents that its use would not infringe privately owned rights. Reference herein to any specific commercial product, process, or service by trade name, trademark, manufacturer, or otherwise, does not necessarily constitute or imply its endorsement, recommendation, or favoring by the United States Government or any agency thereof or its contractors or subcontractors. The views and opinions of authors expressed herein do not necessarily state or reflect those of the United States Government or any agency thereof.

Accelerated degradation in quasi-single-crystalline layered oxide cathode for lithium-ion batteries caused by residual grain boundaries

Rui Zhang $^{1,\parallel}$, Chunyang Wang $^{1,\parallel}$, Mingyuan Ge 2 , and Huolin L. Xin 1*

- 1. Department of Physics and Astronomy, University of California, Irvine, CA 92697, USA.
- 2. National Synchrotron Light Source II, Brookhaven National Laboratory, Upton, NY 11973, USA. || these authors contributed equally to this work
- *Correspondence should be addressed to H.L.X. (huolinx@uci.edu)

Abstract

The rapidly growing demand of electrical vehicle (EV) requires high-energy-density lithium-ion batteries (LIBs) with excellent cycling stability and safety performance. However, conventional polycrystalline high-Ni cathodes severely suffer from intrinsic chemo-mechanical degradation and fast capacity fade. The emerging single-crystallization strategy offers a promising pathway to improve the chemo-mechanical stability, however, the single-crystallinity of the cathode is not always guaranteed and residual grain boundaries (GBs) could persist in nonideal synthesis conditions, leading to the formation of 'quasi' single-crystalline (QSC) cathodes. So far, there is a lack of understanding of the influence of these residual GBs on the electrochemical performance and structural stability. Herein, we investigate the degradation pathway of a QSC high-Ni cathode through transmission electron microscopy and X-ray techniques. The residual GBs caused by insufficient calcination time, dramatically exacerbate the cathode's chemo-mechanical instability and cycling performance. Our work offers important guidance for the next-generation cathodes for long-life LIBs.

Keywords:

Single-crystalline cathode, layered oxide, lithium-ion battery, grain boundary, degradation

Layered oxide cathode with high nickel content (LiNi_{1-x-y}Mn_xCo_yO₂, also noted as NMC), owing to the high specific capacity and high energy density, is considered as the critical material in next-generation Li-ion batteries for electric vehicles¹⁻⁵. Conventional layered oxide cathodes are generally in the form of near-spherical polycrystalline particles (3-10 μm in size) consisting of hundreds of primary particles (100-500 nm in size) tightly packed⁶. However, a consensus regarding this primary-secondary architecture is that the massive interfaces between primary particles facilitate Li⁺ diffusion and

consequently improve the rate performance; while the drawback is equally discouraging--the anisotropic strain during repeated lithiation/delithiation process can easily detach the primary particles from each other, continuously cause the formation of cracks, and lead to severe side reactions⁷⁻¹². Although secondary-particle level coating or doping strategies can significantly enhance capacity retention, it has been proved unsatisfactory in suppressing the intergranular crack formation^{13, 14}. Single-crystallization strategy is considered a promising pathway to suppress the micro-crack formation. Benefiting from the absence of internal grain boundary, the lattice expansion induced anisotropic strain will release at the surface rather than accumulate in the interior^{10, 15, 16}. As a result, the crack formation widely observed at the grain boundaries of conventional polycrystalline cathodes can be intrinsically prohibited, leading to improved capacity retention.

A routine synthesizing process of single-crystalline NMC cathode generally consists of a high-temperature calcination step, followed by a medium-temperature annealing step^{17, 18}. At the high-temperature calcination step, the polycrystalline particle with multiple orientations will rotate, merge, and finally grow to a single-crystalline particle with all the grain boundaries disappeared¹⁹. However, due to the inhomogeneous particle/grain sizes and the randomly distributed orientation of these grains, the grain growth, reorientation, and merge process can be locally non-uniform in non-ideal calcination conditions. This inhomogeneity puts forward an important question that whether some residual grain boundaries potentially persist during the calcination of single-crystalline cathodes. If they exist, how this intermediate state towards ideal single-crystalline cathode will influence the cathode's performance and chemo-mechanical degradation pathways?

Here, as a proof of concept, we designed and synthesized a model cathode sample —a 'quasi' single-crystalline LiNi_{0.8}Mn_{0.1}Co_{0.1}O₂ (NMC-811), and systematically investigated how residual grain boundaries in the 'quasi'-single-crystalline NMC-811 influence the cathode's electrochemical performance and chemomechanical stability. We find that when the calcination time is insufficient, small amounts of GBs still exist in a fraction of the single particles even though the external morphology is similar to the single-crystalline particles. More importantly, these residual GBs significantly accelerated the degradation of surface structure and cycling performance.

Polycrystalline (PC-811), single-crystalline (SC-811), and 'quasi'-single-crystalline that contains a few grains (QSC-811) are synthesized using the same precursor (The electrode is prepared directly after calcination without surface treatment. See details of synthesis in Method). Figure 1a shows the

synthetic routine of different NMC-811 particles by tunning the calcination conditions. Typically, at a relatively low calcination temperature, the grain boundary diffusion is limited, and the corresponding secondary particles are composed of densely packed primary particles ranging from 200-500nm as shown in Figs. 1b and 1e (PC-811); As the calcinated temperature goes higher (900°C), the primary grain will rotate the orientation, merge to large grain with the number of grain boundaries decreased, and finally grow to single-crystalline particles (SC-811) with size ranging from 2-3μm (Figs. 1d and 1g). However, when the calcination time is reduced as shown in Figs. 1c and 1f, although the QSC-811 has a similar particle shape as that of SC-811, FIB cross-section and sample tilting in TEM indicate that these QSC-811 particles still consist of a few grains with different orientations, which means the particle is not fully single-crystallized. Energy dispersive spectroscopy elemental map (EDS mapping) and atomic-resolution high-angle annular dark-field scanning transmission electron microscopy (HAADF-STEM) (Figs. S1-S2) reveal that both SC-811 and QSC-811 has similar elements distribution and the well-ordered *R-3m* layered structure.

Electrochemical performances of SC-811, QSC-811, and PC-811 were evaluated and compared. Figure 2a shows the charge/discharge profile of different types of NMC-811 after two formation cycles. The result shows that the discharge capacity of SC-811 and QSC-811 is 209.5 mAh/g and 212.7 mAh/g, comparable with the 216.6 mAh/g of PC-811. This suggests that by tunning the "two-step" synthesis condition, the SC-811 and QSC-811 cathodes are capable to deliver discharge capacity comparable to the polycrystalline counterpart. However, as a well-known dilemma, as the number of grain boundaries decreases, the rate performance is getting worse owing to the sluggish bulk diffusion. The rate capacity (Fig. S3) shows that at 5C rate current (1C is set to 200mA/g), QSC-811 and SC-811 retain only 61.2% and 64.1% of their discharge capacity at 0.1C respectively, significantly lower than the 69.3% of PC-811. This result is further evidenced by the galvanostatic intermittent titration technique (GITT) measurement shown in Fig. 2c, showing that the Li-ion diffusion constant of PC-811 is slightly higher than that of QSC-811 and SC-811.

Differential capacity (dQdV⁻¹) curves of the initial charge/discharge cycle (Figure 2b) shows that the H2-H3 redox peak intensities in both SC-811 and QSC-811 are reduced compared with PC-811. This result indicates that the detrimental H2-H3 phase transition is to some extent suppressed in SC-811 and QSC-811 compared with PC-811. It's noted that although the H2-H3 redox peak intensity in QSC-811 is close to that of the SC-811, the peak position shifts to a more positive potential, indicating the mitigation of the H2-H3 phase transition during the delithiation of QSC-811. The cycling performances

of the three types of NMC-811 cathodes are evaluated in 2032-type coin cells with Li chips as anodes (2.5V-4.4V, C/3). Figure 2d shows that the capacity retention of SC-811, QSC-811 and PC-811 after 100 cycles are 92.6%, 79.5% and 79.2%, respectively. SC-811 delivers better cycling retention compared with OSC-811 and PC-811, which is in agreement with many reports on single-crystalline NMC cathodes. The Coulombic efficiency (CE) of three types of cathodes are plotted in Fig. S4, showing that the average CE of SC-811, QSC-811 and PC-811 are 99.59%, 99.39% and 99.46%, respectively. The higher CE of SC-811 indicates less side reaction mainly because of the absence of grain boundary. To evaluate the impact of residual GBs on the phase transition during long-term cycling, dQdV⁻¹ curves of SC-811, QSC-811, and PC-811 at different cycling stages are performed. The results in Figs. 2f to 2h show that after 100 cycles, the H2-H3 redox peak of SC-811 remains prominent, while the corresponding redox peaks in both QSC-811 and PC-811 almost disappeared, indicating that more irreversible phase transition occurred during cycling in QSC-811 and PC-811. Moreover, the H2-H3 redox peaks in QSC-811 and PC-811 polarized significantly compared to SC-811 during long-term cycling, suggesting that both QSC-811 and PC-811 suffer higher impedance, which are usually associated with intergranular microcrack formation. Electrochemical impedance spectroscopy (EIS) in Fig. 2e evidenced that after cycling, the impedance behavior in QSC-811 is close to PC-811 rather than SC-811. The above electrochemical performances show that although the residual GBs in the 'quasi'single-crystalline cathode didn't cause serious initial capacity loss, they are prone to promote both the interfacial impedance and irreversible phase transition.

Transmission X-ray microscopes (TXM) tomography combined with SEM (Fig. S5) is applied to better visualize the degradation behavior of these residual GBs. As shown in Figure 3a, 3D reconstruction of a typical secondary particle of PC-811 shows that severe micro-cracks are formed after cycling, in agreement with the increased impedance and polarization in Fig. 2h. As for SC-811, the single-crystalline particles remain intact as shown in Fig. 3c, and no obvious crack forms owing to the absence of internal boundary. Interestingly, in cycled QSC-811 shown in Fig. 3b, a few micro-cracks (usually 2~3 cracks) are observed in a single particle, which is analogous to the crack in PC-811. In general, single-crystalline cathode is proved to be crack-free during cycling because the anisotropic strain will no longer accumulate inside the particles. Nevertheless, these unobtrusive GBs in QSC-811 will lead to the inhomogeneous volume change, which breaks the QSC-811 into several primary particles.

Atomic resolution HAADF-STEM is performed to investigate the origins of increased impedance and polarization in QSC-811. As shown in Fig. 4a, FIB cross-section shows that SC-811 cathode particle

remains uncracked after cycling. Although a rocksalt reconstruction layer is formed on the surface, this layer is relatively thin and uniform with a thickness less than 5nm as shown in Figs. 4b and 4c. In stark contrast, QSC-811 shows distinct and severe cracks after cycling shown in Fig. 4d, matching well with the TXM result. The high-resolution images in Figs. 4e-4f and Fig. S6 show that the surface reconstruction layer around the crack is rather thick (more than 20nm) and disordered, with randomly distributed O1-stacking faults, edge dislocations, and rocksalt phase. Next, AtomSegNet²⁰ software, which is developed by our recent TEM/deep-learning based teniques²¹⁻²³, is employed to perform atomic column localization and segmentation. The super-resolution image in Fig. 4g shows that a large area of O1 stacking faults (highlighted in the upper right panel) along with prominent lattice distortion (lower right panel) are observed in the cycled QSC-811. However, as indicated in Fig. 4h, SC-811 shows much more uniform surface reconstruction after cycling. Despite the thin layer of rocksalt phase and Li/TM interlayer mixing (upper right panel), most of the surface area remains intact R-3m layered structure (lower right panel). Compared with the uniform surface layer in SC-811, QSC-811 shows a much more unfavorable surface reconstruction layer around the crack surface²⁴. It's noted that both the 'pristine surface' of cycled QSC-811 and the surface of cycled PC-811 are also investigated as shown in Fig. S7-S8. The result shows that differ from the crack surface, the reconstruction layer of 'pristine surface' in cycled QSC-811 is more stable with 5-7nm rocksalt layer, while the PC-811 surface consists of thick layer of rocksalt and O1 stacking faults. This unusual surface reconstruction indicates that the residual GBs not only break the intact particle into several primary particles with smaller sizes, more importantly, they also make the fresh surface around the cracks more "vulnerable" compared with the pristine surface. As a result, this thick and disordered surface reconstruction layer remarkably increases the impedance in QSC-811.

Statistical X-ray diffractions (XRD) were performed to show the lattice evolution difference between SC-811 and QSC-811 during cycling. As shown in Fig. 4i, in the pristine particles, QSC-811 and SC-811 shows identical lattice distance in the (003) direction. After cycling the (003) diffraction peak in both QSC-811 and SC-811 shifts to a lower angle, suggesting an expansion of average layered distance. However, in QSC-811, this expansion is more significant than that in SC-811. The expansion along the c axis is mainly attributed to the undesired phase transition during cycling such as rocksalt formation and O1-stacking faults^{25, 26}. In addition to the diffraction peak shift, the (003)/(104) peak intensity ratio ($I_{(003)}/I_{(104)}$) is also compared to evaluate the Li/TM mixing in the layered structure. It can be seen that after long-term cycling, the $I_{(003)}/I_{(104)}$ in QSC-811 ($I_{(003)}/I_{(104)}$ =1.22) is lower than that of SC-811

 $(I_{(003)}/I_{(104)}=1.39)$, indicating that more rocksalt phase is formed in the cycled QSC-811, which is in agreement with the HAADF-STEM results.

Taking the TXM, XRD and STEM results together, it can be inferred that the very few residual GBs can greatly accelerate the degradation of electrochemical performance and structural stability. Although several micro-cracks are observed after cycling in QSC-811, it's unlikely that the increased impedance and the worse capacity retention merely originate from the exposure of fresh surfaces. This is because the newly generated surface area in QSC-811 is significantly less than that of the PC-811. A more destructive impact from the residual GBs is that they destabilize the surface around the crack, leading to a poorer surface structure. It might be attributed to the following reasons: 1) the pristine surface in high-Ni NMC cathode usually shows a thin rocksalt reconstruction layer at the outermost surface during the synthesis, which to some extent passivates the active layered structure and mitigate the continuously attack by electrolyte²⁷. However, compare to the pristine surface, the fresh surface generated from the interior cracks are more likely to be layered structure, promoting the unfavorable chemical delithiation by electrolytes; 2) owing to the presence of several boundaries, the anisotropic stress intends to concentrate. The accumulated strain around the GBs can impel the interlayer slip, the formation of dislocations and stacking faults, which further accelerate the oxygen-loss and phase transformation. As a result, these GBs dramatically exacerbate the structural instability near the surface, leading to performance degradation.

In conclusion, a 'quasi'-single-crystalline NMC-811 cathode, which contains only a few micro-sized grain boundaries in a "single-crystalline"-like particle, is synthesized and compared with traditional polycrystalline NMC-811 and single-crystalline NMC-811. The unobtrusive grain boundaries are directly evidenced by the FIB cross-section image despite single-crystalline morphology. The electrochemical measurements indicate that the few boundaries aggravate the capacity degradation, giving rise to the increased impedance and irreversible phase transformation. The residual grain boundaries not only lead to intergranular cracks but also accelerates the structural degradation of fresh surface, causing a severely disordered surface reconstruction layer. These observations provide new insight into the degradation mechanism of an intermediate cathode architecture between conventional poly-crystalline and single-crystalline cathodes. Our work also suggests that to avoid the rapid capacity degradation in single-crystalline cathode, extra attention should be paid to the potentially existing residual grain boundaries during the general calcination of single-crystalline cathodes.

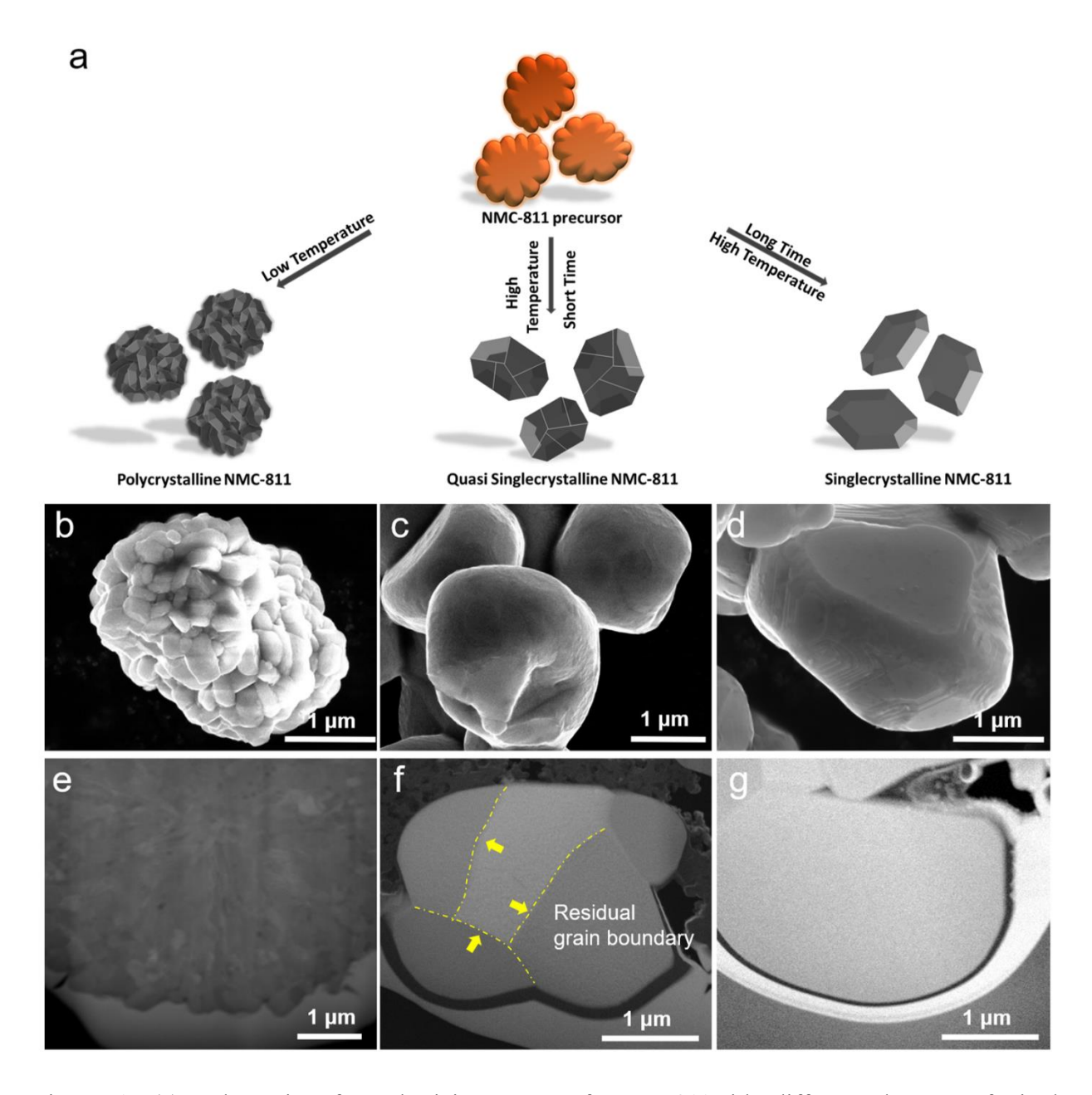


Figure 1. (a) Schematic of synthesizing route of NMC-811with different degrees of single crystallization. (b-d) SEM image of typical morphology of PC-811, QSC-811, and SC-811 particle synthesized from the same precursor, respectively. The particles size of the three cathodes is 2-3μm. (e-g) STEM images of a cross-section of pristine particles of PC-811, QSC-811 and SC-811, respectively. The residual grain boundaries in QSC-811 are indicated by yellow arrows.

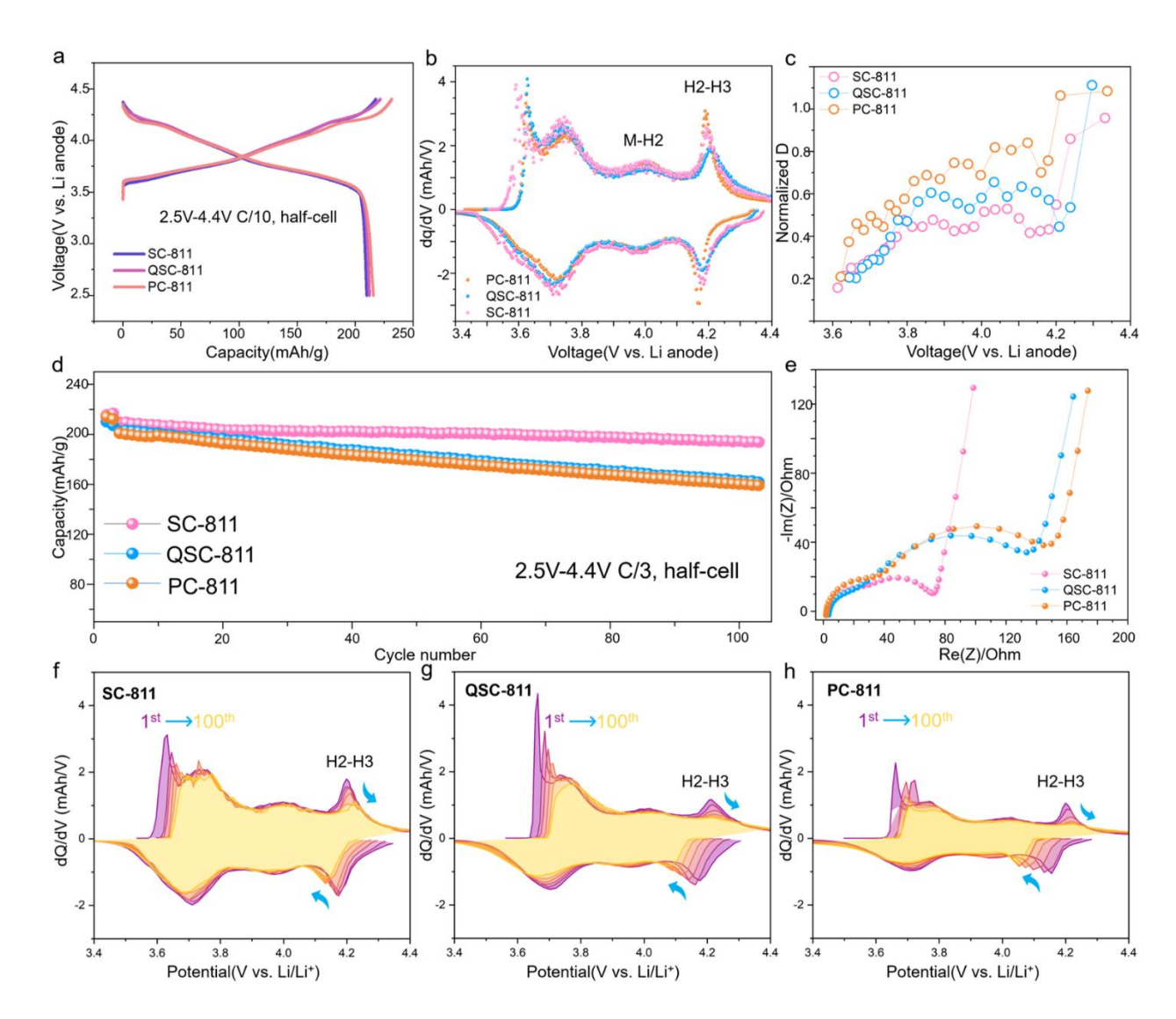


Figure 2. (a) Charge/discharge curve of PC-811, QSC-811 and SC-811, respectively (after formation cycles, 2.5V-4.4V, C/10). (b) Differential capacity (dQdV⁻¹) curves of initial charge/discharge cycle. (c) Relative Li ion diffusion constant of PC-811, QSC-811 and SC-811, respectively. (d) Long term cycling stability (2.5V-4.4V, C/3). (e) EIS curve of half-cell after long term cycling (100mHz to 1MHz). (f-h) dQdV⁻¹ evolution from 1st cycle to 100th cycles in SC-811, QSC-811 and PC-811, respectively.

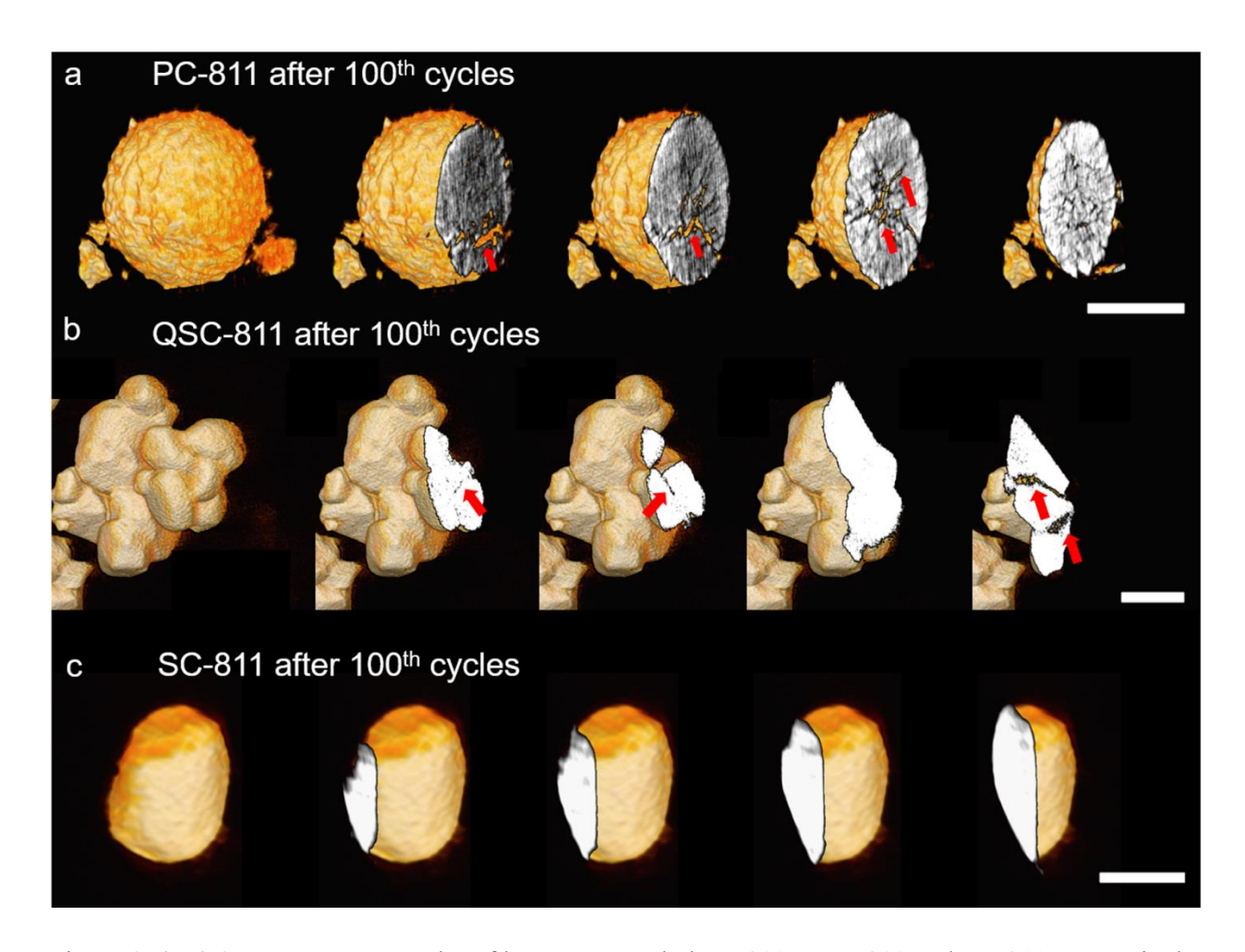


Figure 3. (a-c) 3D TXM tomography of long-term cycled PC-811, QSC-811 and SC-811, respectively, scale bar, $2\mu m$. The results indicate that $2\sim3$ micro-sized cracks are formed in QSC-811, while the interior of SC-811 remains uncracked.

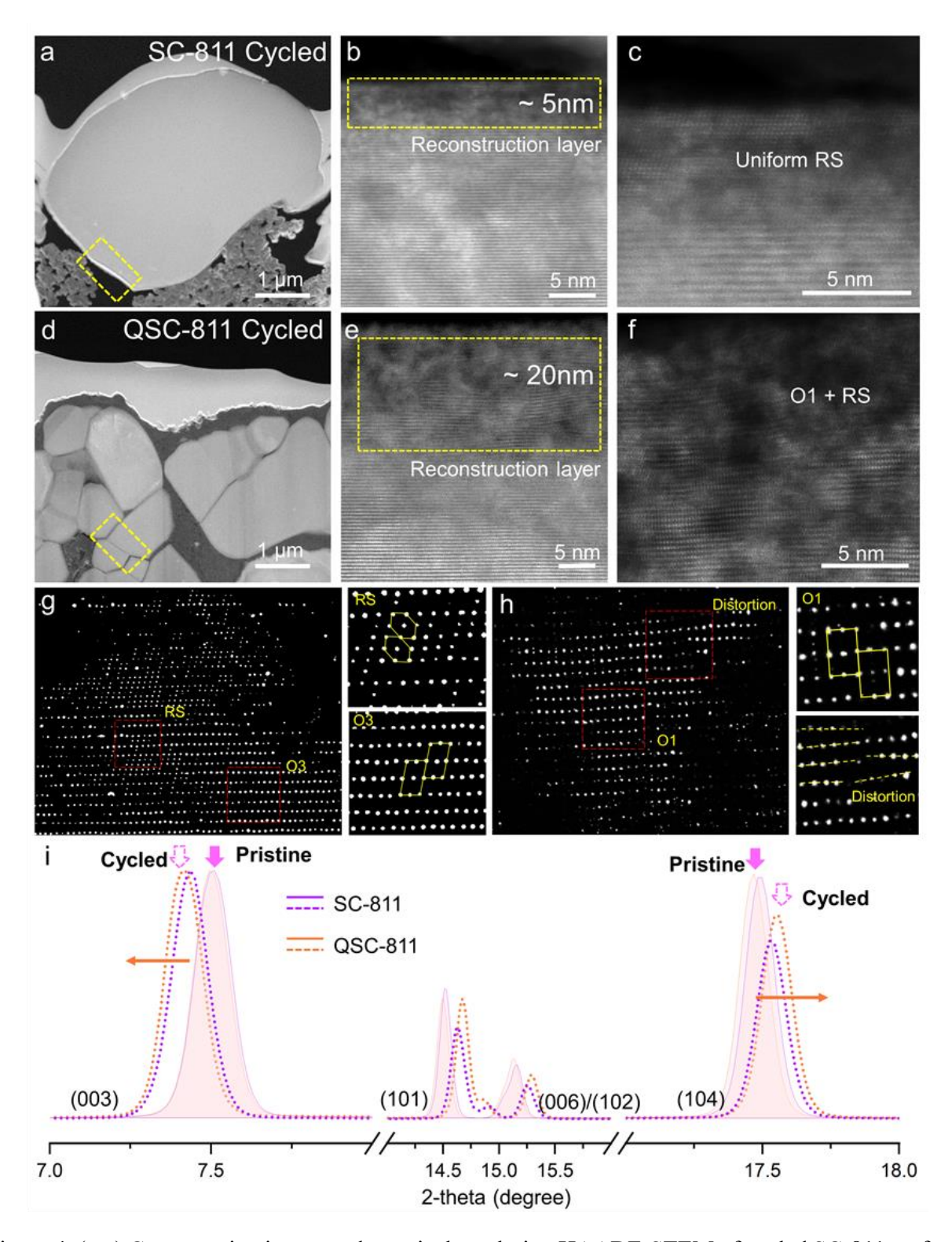


Figure 4. (a-c) Cross-section image and atomical resolution HAADF-STEM of cycled SC-811 surface. (d-f) Cross-section image and atomical resolution HAADF-STEM of cycled QSC-811 surface. (g-h)

Super-resolution image corresponding to the (c) and (f) obtained by AtomSegNet processing. (i) XRD

comparison of SC-811 and QSC-811 before and after cycling (Pristine: solid line; Cycled: dashed line).

ASSOCIATED CONTENT

Supporting information

Method, cross-section EDS mapping of pristine SC-811 and QSC-811, atomic resolution HAADF-

STEM of pristine SC-811 and QSC-811, rate performance, CE, SEM image of long-term cycled SC-

811, QSC-811 and PC-811 particles, and atomic resolution HAADF-STEM images of PC-811 and

QSC-811 surface layer (PDF).

AUTHOR INFORMATION

Corresponding Authors

*E-mail: huolinx@uci.edu

Author contributions

H.L.X. conceived and directed the project. R.Z. synthesized the materials and performed the

electrochemical experiments. C.Y.W. performed the TEM experiments and data analyses. C.Y.W. and

M.Y.G. conducted the TXM experiments and data analysis. R.Z. and C.Y.W. wrote the paper with help

from all authors.

Notes

The authors declare no competing financial interest.

ACKNOWLEDGMENT

This research was primarily supported by the Early Career Research Program, Materials Science and

Engineering Divisions, Office of Basic Energy Sciences of the U.S. Department of Energy, under

award no. DE-SC0021204 and additional support for synthesis received from the U.S. Department of

Energy Office of Energy Efficiency and Renewable Energy under the award number DE-EE0008444.

R.Z. was funded by H.L.X.'s startup funding provided by UC Irvine. The authors acknowledge the use

of facilities and instrumentation at the UC Irvine Materials Research Institute (IMRI), which is supported in part by the National Science Foundation through the UC Irvine Materials Research Science and Engineering Center (DMR-2011967). This research used resources of the Center for Functional Nanomaterials, which is a U.S. DOE Office of Science Facility, at Brookhaven National Laboratory under contract no. DESC0012704. This research used 7-BM of the National Synchrotron Light Source II, a U.S. Department of Energy (DOE) Office of Science User Facility operated for the DOE Office of Science by Brookhaven National Laboratory under Contract No. DE-SC0012704. We acknowledge Kim Kisslinger and Lu Ma at BNL for the collaboration of preparing samples and measurements.

REFERENCES

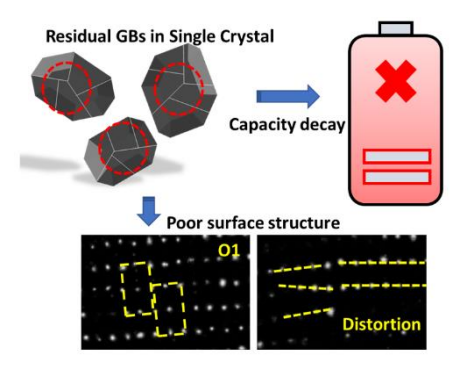
- 1. Li, W.; Erickson, E. M.; Manthiram, A., High-nickel layered oxide cathodes for lithium-based automotive batteries. *Nature Energy* **2020**, *5* (1), 26-34.
- 2. Lin, R.; Bak, S.-M.; Shin, Y.; Zhang, R.; Wang, C.; Kisslinger, K.; Ge, M.; Huang, X.; Shadike, Z.; Pattammattel, A.; Yan, H.; Chu, Y.; Wu, J.; Yang, W.; Whittingham, M. S.; Xin, H. L.; Yang, X.-Q., Hierarchical nickel valence gradient stabilizes high-nickel content layered cathode materials. *Nature Communications* **2021**, *12* (1), 2350.
- 3. Liu, T.; Yu, L.; Liu, J.; Lu, J.; Bi, X.; Dai, A.; Li, M.; Li, M.; Hu, Z.; Ma, L.; Luo, D.; Zheng, J.; Wu, T.; Ren, Y.; Wen, J.; Pan, F.; Amine, K., Understanding Co roles towards developing Co-free Ni-rich cathodes for rechargeable batteries. *Nature Energy* **2021**, *6* (3), 277-286.
- 4. Lin, R.; Hu, E.; Liu, M.; Wang, Y.; Cheng, H.; Wu, J.; Zheng, J.-C.; Wu, Q.; Bak, S.; Tong, X.; Zhang, R.; Yang, W.; Persson, K. A.; Yu, X.; Yang, X.-Q.; Xin, H. L., Anomalous metal segregation in lithium-rich material provides design rules for stable cathode in lithium-ion battery. *Nature Communications* **2019**, *10* (1), 1650.
- 5. Lin, F.; Nordlund, D.; Weng, T.-C.; Zhu, Y.; Ban, C.; Richards, R. M.; Xin, H. L., Phase evolution for conversion reaction electrodes in lithium-ion batteries. *Nature Communications* **2014**, *5* (1), 3358.
- 6. Maeng, S.; Chung, Y.; Min, S.; Shin, Y., Enhanced mechanical strength and electrochemical performance of core—shell structured high—nickel cathode material. *Journal of Power Sources* **2020**, *448*, 227395.
- 7. Trevisanello, E.; Ruess, R.; Conforto, G.; Richter, F. H.; Janek, J., Polycrystalline and Single Crystalline NCM Cathode Materials—Quantifying Particle Cracking, Active Surface Area, and Lithium Diffusion. *Advanced Energy Materials* **2021**, *11* (18), 2003400.
- 8. Wang, C.; Han, L.; Zhang, R.; Cheng, H.; Mu, L.; Kisslinger, K.; Zou, P.; Ren, Y.; Cao, P.; Lin, F.; Xin, H. L., Resolving atomic-scale phase transformation and oxygen loss mechanism in ultrahigh-nickel layered cathodes for cobalt-free lithium-ion batteries. *Matter* **2021**, *4* (6), 2013-2026.
- 9. Wang, C.; Zhang, R.; Kisslinger, K.; Xin, H. L., Atomic-Scale Observation of O1 Faulted Phase-Induced Deactivation of LiNiO2 at High Voltage. *Nano Letters* **2021**, *21* (8), 3657-3663.
- 10. Wang, C.; Zhang, R.; Siu, C.; Ge, M.; Kisslinger, K.; Shin, Y.; Xin, H. L., Chemomechanically Stable Ultrahigh-Ni Single-Crystalline Cathodes with Improved Oxygen Retention and Delayed Phase Degradations. *Nano Letters* **2021**, *21* (22), 9797-9804.

- 11. Yan, P.; Zheng, J.; Gu, M.; Xiao, J.; Zhang, J.-G.; Wang, C.-M., Intragranular cracking as a critical barrier for high-voltage usage of layer-structured cathode for lithium-ion batteries. *Nature Communications* **2017**, *8* (1), 14101.
- 12. Li, J.; Cameron, A. R.; Li, H.; Glazier, S.; Xiong, D.; Chatzidakis, M.; Allen, J.; Botton, G. A.; Dahn, J. R., Comparison of Single Crystal and Polycrystalline LiNi0.5Mn0.3Co0.2O2Positive Electrode Materials for High Voltage Li-lon Cells. *Journal of The Electrochemical Society* **2017**, *164* (7), A1534-A1544.
- 13. Herzog, M. J.; Esken, D.; Janek, J., Improved Cycling Performance of High-Nickel NMC by Dry Powder Coating with Nanostructured Fumed Al2O3, TiO2, and ZrO2: A Comparison. *Batteries & Supercaps* **2021**, *4* (6), 1003-1017.
- 14. Sun, H. H.; Ryu, H.-H.; Kim, U.-H.; Weeks, J. A.; Heller, A.; Sun, Y.-K.; Mullins, C. B., Beyond Doping and Coating: Prospective Strategies for Stable High-Capacity Layered Ni-Rich Cathodes. *ACS Energy Letters* **2020**, *5* (4), 1136-1146.
- 15. Bi, Y.; Tao, J.; Wu, Y.; Li, L.; Xu, Y.; Hu, E.; Wu, B.; Hu, J.; Wang, C.; Zhang, J.-G.; Qi, Y.; Xiao, J., Reversible planar gliding and microcracking in a single-crystalline Ni-rich cathode. *Science* **2020**, *370* (6522), 1313-1317.
- 16. Fan, X.; Hu, G.; Zhang, B.; Ou, X.; Zhang, J.; Zhao, W.; Jia, H.; Zou, L.; Li, P.; Yang, Y., Crack-free single-crystalline Ni-rich layered NCM cathode enable superior cycling performance of lithium-ion batteries. *Nano Energy* **2020**, *70*, 104450.
- 17. Li, H.; Li, J.; Zaker, N.; Zhang, N.; Botton, G. A.; Dahn, J. R., Synthesis of Single Crystal LiNi0.88Co0.09Al0.03O2 with a Two-Step Lithiation Method. *Journal of The Electrochemical Society* **2019**, *166* (10), A1956-A1963.
- 18. Liu, A.; Zhang, N.; Stark, J. E.; Arab, P.; Li, H.; Dahn, J. R., Synthesis of Co-Free Ni-Rich Single Crystal Positive Electrode Materials for Lithium Ion Batteries: Part I. Two-Step Lithiation Method for Al- or Mg-Doped LiNiO2. *Journal of The Electrochemical Society* **2021**, *168* (4), 040531.
- 19. Wang, T.; Ren, K.; He, M.; Dong, W.; Xiao, W.; Pan, H.; Yang, J.; Yang, Y.; Liu, P.; Cao, Z.; Ma, X.; Wang, H., Synthesis and Manipulation of Single-Crystalline Lithium Nickel Manganese Cobalt Oxide Cathodes: A Review of Growth Mechanism. *Front Chem* **2020**, *8*, 747.
- 20. Lin, R.; Zhang, R.; Wang, C.; Yang, X.-Q.; Xin, H. L., TEMImageNet training library and AtomSegNet deep-learning models for high-precision atom segmentation, localization, denoising, and deblurring of atomic-resolution images. *Scientific Reports* **2021**, *11* (1), 5386.
- 21. Zheng, S.; Wang, C.; Yuan, X.; Xin, H. L., Super-compression of large electron microscopy time series by deep compressive sensing learning. *Patterns* **2021**, *2* (7), 100292.
- Wang, C.; Ding, G.; Liu, Y.; Xin, H. L., 0.7 Å Resolution Electron Tomography Enabled by Deep-Learning-Aided Information Recovery. *Advanced Intelligent Systems* **2020**, *2* (12), 2000152.
- 23. Ding, G.; Liu, Y.; Zhang, R.; Xin, H. L., A joint deep learning model to recover information and reduce artifacts in missing-wedge sinograms for electron tomography and beyond. *Scientific Reports* **2019**, *9* (1), 12803.
- 24. Lin, F.; Markus, I. M.; Nordlund, D.; Weng, T.-C.; Asta, M. D.; Xin, H. L.; Doeff, M. M., Surface reconstruction and chemical evolution of stoichiometric layered cathode materials for lithium-ion batteries. *Nature Communications* **2014**, *5* (1), 3529.
- 25. Li, W.; Liu, X.; Xie, Q.; You, Y.; Chi, M.; Manthiram, A., Long-Term Cyclability of NCM-811 at High Voltages in Lithium-Ion Batteries: an In-Depth Diagnostic Study. *Chemistry of Materials* **2020**, *32* (18), 7796-7804.
- 26. Xu, C.; Märker, K.; Lee, J.; Mahadevegowda, A.; Reeves, P. J.; Day, S. J.; Groh, M. F.; Emge, S. P.; Ducati, C.; Layla Mehdi, B.; Tang, C. C.; Grey, C. P., Bulk fatigue induced by surface reconstruction in layered Ni-rich cathodes for Li-ion batteries. *Nature Materials* **2021**, *20* (1), 84-92.

27. Zou, L.; He, Y.; Liu, Z.; Jia, H.; Zhu, J.; Zheng, J.; Wang, G.; Li, X.; Xiao, J.; Liu, J.; Zhang, J.-G.; Chen, G.; Wang, C., Unlocking the passivation nature of the cathode—air interfacial reactions in lithium ion batteries. *Nature Communications* **2020**, *11* (1), 3204.

Accelerated degradation in quasi-single-crystalline layered oxide cathode for lithium-ion batteries caused by residual grain boundaries

Rui Zhang $^{1,\,\parallel},$ Chunyang Wang $^{1,\,\parallel},$ Mingyuan Ge², and Huolin L. Xin 1*



TOC Figure